


Communication

Composites of Laminar Nanostructured ZnO and VOx-Nanotubes Hybrid as Visible Light Active Photocatalysts

Eglantina Benavente ^{1,*} , Daniel Navas ¹, Sindy Devis ¹, Marjorie Segovia ², Clivia Sotomayor-Torres ^{3,4} and Guillermo González ^{2,5}

¹ Departamento de Química, Universidad Tecnológica Metropolitana, P.O. Box 9845, Santiago, Chile; daniel.navas@utem.cl (D.N.); sdevis@utem.cl (S.D.)

² Department of Chemistry, Faculty of Sciences, Universidad de Chile, P.O. Box 653, Santiago, Chile; msmonrroy@gmail.com (M.S.); ggonzale@uchile.cl (G.G.)

³ Catalan Institute of Nanoscience and Nanotechnology (ICN2), CSIC and BIST, Campus UAB Bellaterra, 08193 Barcelona, Spain; clivia.sotomayor@icn2.cat

⁴ ICREA, Pg. Lluís Companys 23, 08010 Barcelona, Spain

⁵ Center for the Development of Nanoscience and Nanotechnology, CEDENNA, Av. Ecuador 3493, Santiago, Chile

* Correspondence: ebenaven@utem.cl; Tel.: +56-227877109

Received: 15 January 2018; Accepted: 15 February 2018; Published: 24 February 2018

Abstract: A series of hybrid heterostructured nanocomposites of ZnO with V₂O₅ nanotubes (VOx-NTs) in different mixing ratios were synthesized, with the aim of reducing the recombination of photoinduced charge carriers and to optimize the absorption of visible light. The study was focused on the use of heterostructured semiconductors that can extend light absorption to the visible range and enhance the photocatalytic performance of ZnO in the degradation of methylene blue as a model pollutant. The addition of VOx-NTs in the synthesis mixture led to a remarkable performance in the degradation of the model dye, with hybrid ZnO (stearic acid)/VOx-NTs at a ratio of 1:0.06 possessing the highest photocatalytic activity, about seven times faster than pristine zinc oxide. Diffuse reflectance spectroscopic measurements and experiments in the presence of different trapping elements allowed us to draw conclusions regarding the band positions and photocatalytic degradation mechanism. The photocatalytic activity measured in three subsequent cycles showed good reusability as no significant loss in efficiency of dye degradation was observed.

Keywords: ZnO nanocomposites; VOx nanotubes; visible light photocatalyst; methylene blue degradation

1. Introduction

The use of nanostructured inorganic semiconductors for generating chemical energy through photocatalytic processes is of considerable interest. The fundamental and applied research in recent decades focused on wide band-gap semiconductors has proven these materials to be promising for green technology in the development of environmental purification [1,2]. Oxide semiconductors, such as TiO₂ and more recently ZnO, have been proven as efficient photocatalysts for photocatalytic degradation of organic pollutants and photocatalytic water splitting [3,4]. In recent years, nanostructured ZnO, with a wide direct band gap of ~3.2 eV, has been recognized as a significant photocatalytic material, owing to its high photostability and photosensitivity, low cost, non-toxic nature, and high exciton binding energy of 60 meV. Similar to other wide band-gap semiconductors, ZnO is restricted to ultraviolet (UV) excitation only, and fast recombination of photogenerated charge carriers limits its practical applications [5–7]. Thus, the development of visible-light-driven photocatalysts has

recently become a very important topic of research. An effective approach to increase semiconductor photoactivity in visible light is by combining them with other semiconductors with small band gaps, which can be expected to enhance the photocatalytic degradation of organic contaminants under visible-light irradiation. For example, SnO_2/ZnO [8], TiO_2/ZnO [9] and WO_3/ZnO [10] composite heterostructures appear to be very efficient for the photodecomposition of organic dyes. So far, a great number of semiconductors with narrow bandgaps, such as BiOI, CuInS_2 , CuO and V_2O_5 , loaded on the surface of ZnO, have been investigated for the design of visible-light-driven composite photocatalysts [11–14]. Thus, the designed heterostructure of different nanostructured semiconductors in the form of nanocomposites augments the performance by mutual separation/transfer of charge carriers from one semiconductor to another, which can solve the two main drawbacks of ZnO photocatalysts simultaneously, namely, recombination and optimization of the absorption to improve the photocatalytic activity.

As alternative visible-light sensitizers, V_2O_5 semiconductors have recently received much attention because they have a high light absorption coefficient, an appropriate bandgap and are environmentally non-toxic. In particular, vanadium oxide nanotubes ($\text{VO}_x\text{-NTs}$) with a nanotubular morphology have attracted significant attention because of their considerable interest for numerous potential applications in catalysis and devices in batteries [15,16]. In turn, V_2O_5 nanotubular materials formed of multiwall tubular nanostructures of mixed valence V^{4+} and V^{5+} ions with hexadecylamine as templated are expected to have unusual characteristics, amplified by their marked shape-specific, quantum size effects, large active surface area and improved crystallinity [17,18]. For a given semiconductor, the photocatalytic performance in general increases with increasing particle aspect ratio. The photocatalytic efficiency attained with nanotubes architecture, normally higher than with particulate architecture, would arise from a reduction of electron-hole recombination rates promoted by higher charge delocalization along nanotube main axis larger electron mean free path [19]. These properties could induce the collection of photogenerated electrons and holes on the semiconductor surface, optimizing the absorption in the visible region and enhancing the redox reactions of the electrons and holes, thereby increasing their potential use as sensitizers in the degradation of pollutants.

In this study, we successfully synthesized and evaluated the photocatalytic activity of heterostructured nanocomposites formed by laminar hybrid ZnO constituted of single nanosheets sandwiched between self-assembled carboxylic acid monolayers and $\text{VO}_x\text{-NTs}$ in different mixing ratios. The series of nanocomposites are ZnO (stearic acid)/ $\text{VO}_x\text{-NTs}$ in various molar ratios of 1:0.12, 1:0.06 and 1:0.03, respectively. The photocatalytic performance of all the prepared catalysts in decolorization reactions was then evaluated in the degradation of methylene blue (MB), used as a model polluting dye under solar simulated light. The results reveal that ZnO (stearic acid)/ $\text{VO}_x\text{-NTs}$ with a ratio of 1:0.06 were found to be optimal and possessed the highest photocatalytic activity of all the investigated samples, seven times higher than ZnO under visible light following pseudo first-order kinetics. Scavengers were used for understanding of the photocatalytic degradation mechanisms of dye in the presence of heterostructured nanocomposites and visible irradiation. Moreover, after each photocatalysis reaction, the photocatalyst was reused at least three times without any obvious change in efficiency and properties.

2. Results and Discussion

The X-ray diffraction (XRD) patterns of the synthesized nanocomposites are shown in Figure 1. The lamellar nature of ZnO (stearic acid) is confirmed by its XRD pattern (Figure 1a), which displays low-angle reflections characteristic of well-ordered laminar arrangements, according to the positions of the (001) reflections in the diffraction pattern and the interlayer distances along the c-axis. The reflections at higher angles indicate the nanocomposite inorganic moiety correspond to a ZnO single phase with the wurtzite structure (JCPDS 36-1451). For $\text{VO}_x\text{-NTs}$, the pattern given in Figure 1b corresponds to the well-ordered lamellar structure of the tubular samples, showing a set of multi-order (001) reflections of the V_2O_5 phase with higher interplanar spacings that correspond

to the two-dimensional structure of VOx layers (Table S1). The diffraction pattern of ZnO (stearic acid)/VOx-NTs (Figure 1c) was indexed the phase ZnO and well-defined ZnO (stearic acid) layered phases. No obvious changes were observed in the XRD pattern after adding VOx-NTs, probably due to the low concentration (<5%) of the latter. In this XRD pattern, no other possible impurities were detected, which suggested that the nanocomposites remained unaltered.

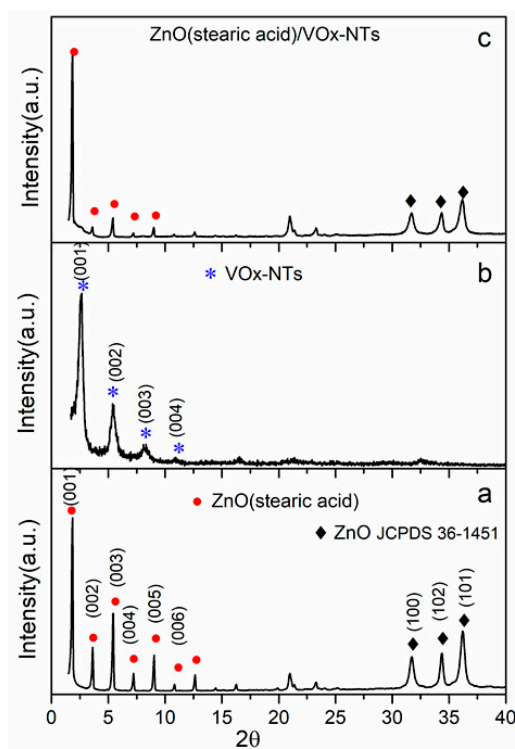


Figure 1. XRD patterns of (a) ZnO (stearic acid), (b) VOx-NTs and (c) nanocomposite hybrid ZnO/VOx-NTs. The peak positions in the reference diffraction pattern of ZnO are also indicated.

The morphology of the studied nanocomposites is illustrated in the micrographs in Figure 2. The Transmission Electron Microscopy (TEM) image in Figure 2a shows the layered nature of ZnO (stearic acid) with sheets. Figure 2b shows the micrograph highlighting the uniform tubular nature of the V₂O₅ nanotubes, composed of vanadate atomic layers and hollow centers. The scanning electron microscopy (SEM) image in Figure 2c present nanotubes of vanadium oxide. The SEM image in Figure 2d shows the heterostructure of ZnO (stearic acid)/VOx-NTs, consisting predominately of sheets of the nanocomposite with tubes of vanadium oxide. The Energy Dispersive X-ray spectroscopy (EDS) patterns in Figure 2e confirm the presence of all constituent elements (Zn, O and V), with no other significant impurities observed. The TEM image in Figure 2f shows the heterostructure of the ZnO (stearic acid) and VOx-NT combination. The lamellar nature of ZnO (stearic acid) and the nanotubes was retained in the composites.

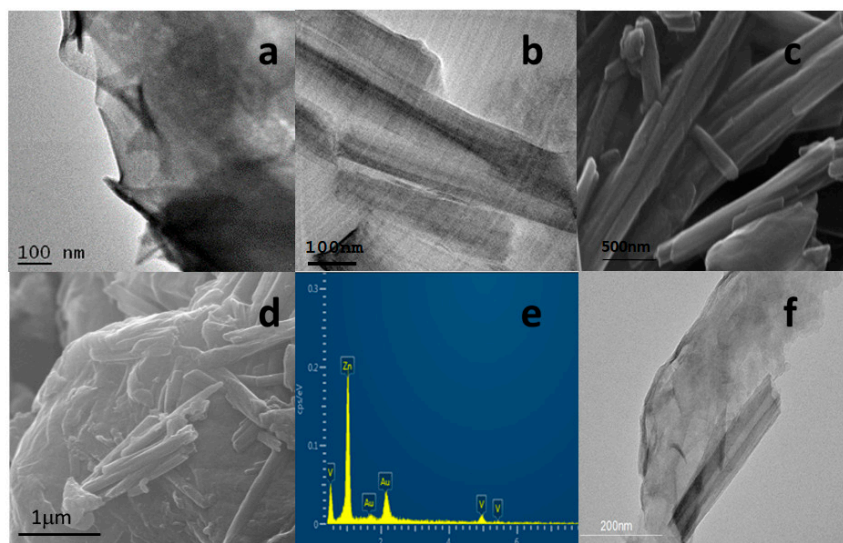


Figure 2. (a) TEM image of ZnO (stearic acid), (b) TEM image of VOx-NTs, (c) SEM image of VOx-NTs, (d) SEM image of nanocomposite ZnO (stearic acid)/VOx-NTs, (e) EDS of nanocomposite and (f) TEM image of nanocomposite ZnO (stearic acid)/VOx-NTs.

UV-vis diffuse reflectance spectroscopy (DRS) was employed to characterize the optical properties in the range of 200–800 nm of all prepared samples. The optical absorption of all semiconductor materials is directly affected by their electronic band gap structure, which determines the photocatalytic activity of the materials. The band gap energy of ZnO (stearic acid), VOx-NTs and of ZnO (stearic acid)/VOx-NTs was estimated using Tauc plots and the extrapolation of the linear slope to photon energy, as shown in Figure 3. The estimated band gap energies of ZnO (stearic acid) and VOx-NTs were ~3.25 and ~2.40 eV, respectively, and the band gap of the ZnO (stearic acid)/VOx-NTs nanocomposites is the combination of both estimated band gaps [20]. Their broad absorbance in the UV to visible window clearly demonstrates that ZnO (stearic acid)/VOx-NTs nanocomposites become photoactive in both the UV and visible light region, which is crucial for full use of sunlight in photocatalysis, which may allow more visible light absorption, hence improving the photocatalytic activity.

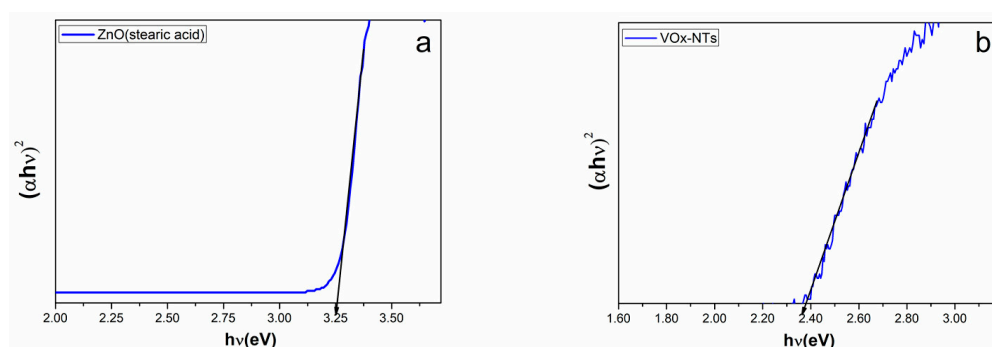


Figure 3. Cont.

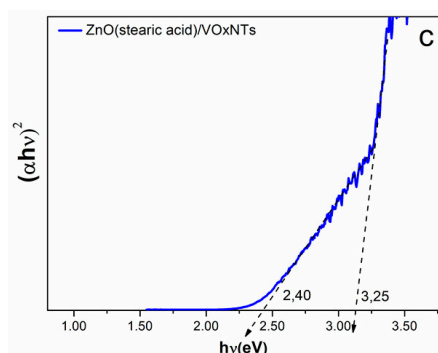


Figure 3. Tauc plots of indirect band gap determination of (a) ZnO (stearic acid), (b) VOx-NTs and (c) nanocomposite hybrid ZnO/VOx-NTs.

The photocatalytic activity of the nanocomposites was studied for the degradation of MB as a pollutant model with visible-light irradiation. During the photochemical reaction, the adsorption of dye over the photocatalyst is an important phenomenon to analyze before photocatalysis. Thus, the dye solution along with the catalyst was kept in the dark in a buffer solution (pH 7) with rigorous stirring for 30 min to establish adsorption equilibrium. To further investigate the photocatalytic behavior of the hybrid ZnO/VOx-NTs, various molar compositions were prepared mechanically by mixing components under sonication. To demonstrate the influence of each of the samples in the photodegradation of the dye, the pure ZnO, ZnO (stearic acid), VOx-NTs and heterostructure hybrid samples were studied under solar simulated light. Figure 4a shows the variation of C/C_0 with time. The photocatalytic properties of the as-prepared samples were evaluated under similar conditions and all curves were normalized after reaching the adsorption/desorption equilibrium. The results show the photocatalytic efficiency of the samples of different compositions. The maximum photocatalytic activity was achieved with heterostructure hybrid ZnO (stearic acid)/VOx-NTs at a ratio of 1:0.06 after 210 min of visible-light irradiation, with the photodegradation efficiency of MB at ~80%. However, the hybrid ZnO/VOx-NTs with a ratio of 1:0.12 showed lower photocatalytic ability than the other samples, which could be attributed to the higher concentration of VOx-NTs, acting as recombination centers for photogenerated charge carriers and increasing the sample opacity, obstructing the light absorption, and decreasing the photocatalytic activity [21]. In this work, the photocatalytic degradation of MB could be described by pseudo-first-order kinetics, $\ln(C/C_0) = kt$, where k is the corresponding kinetic constant and t is the irradiation time. The kinetic rate constant can be obtained from the linear plot of $-\ln(C/C_0)$ with t [22]. The slope obtained gives the apparent rate constant k_{app} in min^{-1} (Figure 4b). The apparent rate constants of hybrid ZnO (stearic acid)/VOx-NTs with a ratio of 1:0.06 were about seven times higher than for ZnO. The rate constants were calculated together with the linear regression coefficients (R^2) for all samples under solar simulated light. These results agreed qualitatively with reports on the photocatalytic efficiency improvement of layered hybrids [23].

The UV-vis spectrum of MB remained practically unaltered during the process and no organic subproducts were detected, thus suggesting mineralization of the dye (Figure 4c). The possible mechanism for the photocatalytic degradation of MB is proposed and presented, showing the charge separation and transfer activity in the nanostructured system. The potential of the positions, the conduction band (CB) and valence band (VB) for hybrid ZnO and VOx-NTs were calculated by applying the empirical equations reported in the literature, where E_{VB} is the VB edge potential, χ is the electronegativity of the semiconductor, which is the geometric mean of the electronegativity of the constituent atoms (χ values for ZnO and V_2O_5 are ca. 5.79 and 6.00 eV, respectively), E^e is the energy of free electrons on the hydrogen scale (~4.5 eV) and E_g is the band gap energy of the semiconductor calculated from DRS data [24].

$$E_{CB} = \chi - E^e - 0.5E_g$$

$$E_{VB} = E_{CB} + E_g$$

The photoinduced charge transfer across the heterojunction is based on the CB edge potential of hybrid ZnO (-0.33 eV vs. NHE) and of VO_x-NTs (0.30 eV vs. NHE). The schematic under visible-light irradiation is illustrated in Figure 4d. The electrons can be excited to the CB of hybrid ZnO, leaving holes in the VB react with OH[−] on the catalyst surface to form \bullet OH radicals. Because the potential of VO_x-NTs ($E_{CB} = 0.30$ eV) is lower than the CB level of hybrid ZnO ($E_{CB} = -0.33$ V), the photogenerated CB electrons in the hybrid ZnO can transfer to VO_x-NTs and then effectively reduce partial V⁵⁺ to V⁴⁺, thus promoting the separation and transfer of photogenerated electron/hole pairs [25,26].

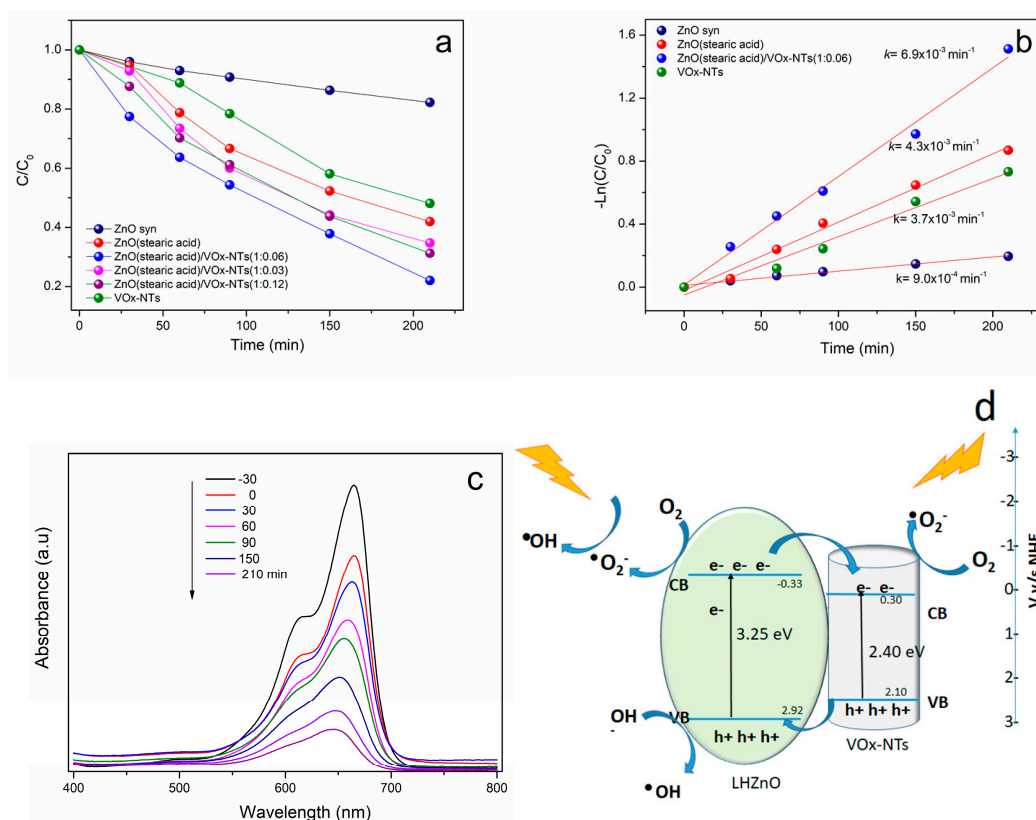


Figure 4. (a) Photocatalytic degradation of MB under visible light of samples, (b) photodegradation kinetics of MB over samples, (c) UV-vis degradation of MB ZnO (stearic acid)/VO_x-NTs 1:0.06 and (d) schematic illustration of the photocatalytic mechanism of ZnO (stearic acid)/VO_x-NTs.

In addition, one more factor that significantly influences the photocatalytic activity involves the redox reactions on the photocatalyst surface, where organic pollutants would be eventually degraded through photocatalytic oxidation by some reactive species. The photocatalytic degradation of MB by the photocatalyst was carried out with the addition of different quenchers under visible-light irradiation, and the results of the trapping experiments are given in Figure 5a. It can be seen that the photodegradation efficiency of MB with the addition of isopropanol (a hydroxyl radical (\bullet OH) scavenger, 2 mM) and chloroform (a superoxide radical ($\text{O}_2^{\bullet-}$) scavenger, 2 mM) was slightly decreased compared to those without the addition of quenchers. The addition of ammonium oxalate (a hole scavenger, 2 mM) did not show changes in the MB photodegradation activity [27,28]. The result of the scavenging test with chloroform and isopropanol are as seen, the removal efficiency of MB within 140 min of reaction time was decreased from 62.3% in the absence of the scavenger to 52.7% and 44.0%, respectively. This study demonstrates that $\text{O}_2^{\bullet-}$ plays an active role in the MB degradation and \bullet OH is the dominant reactive oxygen species responsible for MB degradation and deduced that the radicals \bullet OH and $\text{O}_2^{\bullet-}$ are the species primarily responsible for photocatalytic oxidative reactions.

The production process of radical superoxide and hydroxyl are favored in the conduction bands. The results obtained agree with the positions of the bands determined by applying the empirical equations previously discussed.

We also investigated the stability of the photocatalyst. Catalyst lifetime is an important parameter of the photocatalytic process because of its use for a longer period of time, for this reason, the photocatalyst ZnO (stearic acid)/VOx-NTs was recycled over three cycles for a period of 210 min irradiation. Figure 5b clearly shows a loss of 5% in each study of photocatalytic activity, which might be due to the loss of the photocatalyst during each cycle of reusability.

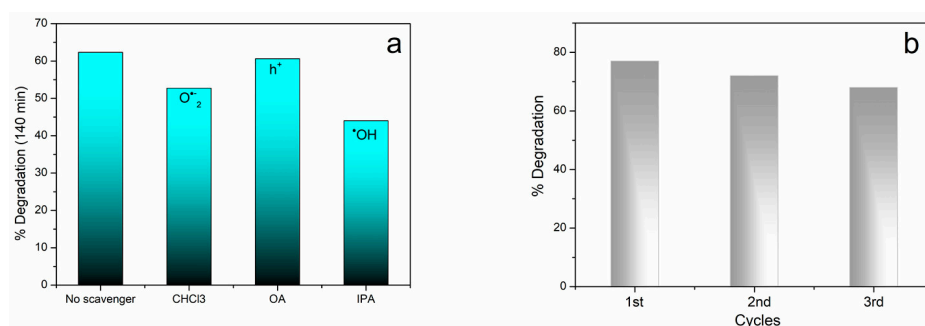


Figure 5. (a) Photocatalytic degradation of MB under solar simulated light after addition of several trapping reagents and (b) recycled test of MB photodegradation under solar simulated light of ZnO (stearic acid)/VOx-NTs 1:0.06.

The efficacy of the products described as photocatalysts for the photo-oxidation of organic pollutants is associated with the presence of organic surfactant in the interlaminar spaces and the surface properties of layered hybrid nanocomposites with nanotubes, which provide more reaction sites for the adsorption of pollutants, enhanced effective electron/hole separation and defects arising in the semiconductor interfaces.

3. Materials and Methods

3.1. Materials

All the reagents in this study were commercial products and were used without any purification. The reagents were purchased from Sigma-Aldrich and Merck (St. Louis, MO, USA). Nanopure water was obtained from a water purification system.

3.2. Synthesis of ZnO (Stearic Acid)

In a typical procedure, ZnSO₄ (1 mol L⁻¹) was mixed with Na₂CO₃ (1 mol L⁻¹)/NaOH (1 mol L⁻¹) (1:1) to afford a ZnO hydrogel. Then, a stearic acid 4.0 × 10⁻¹ mol L⁻¹ aqueous solution was added to the ZnO hydrogel solution under stirring at room temperature; the suspension was stirred at 60 °C followed by an aging period of 24 h at room temperature. The thus formed white precipitate was separated by centrifugation, washed with water/acetone (1:1) mixture, dried at 80 °C for 72 h [29].

3.3. Synthesis of Vanadium Oxide Nanotubes

A solution of 10⁻³ mol of hexadecylamine in pure ethanol, previously degassed, was mixed with 2 × 10⁻³ mol of vanadium triisopropoxide. The yellow solution, obtained after vigorous stirring in an argon atmosphere for 1 h, was then hydrolyzed by adding 15 mL of water. The orange suspension obtained after stirring for 24 h was subjected to a hydrothermal treatment in a Teflon-lined autoclave at 180 °C for 6 days. The resulting black solid was separated, washed with pure ethanol and water, and dried at 80 °C for 72 h [30].

3.4. Photocatalytic Experiments

The photocatalytic activity of the products was evaluated by measuring the degradation of MB in water. For this study, the characteristic absorption peak of MB at 665 nm was monitored using a UV-vis spectrophotometer. The nanocomposite ZnO (stearic acid) (10 mg) was mixed mechanically with VOx-NTs in different proportions in 25 mL of a 1×10^{-5} mol L⁻¹ in phosphate buffer solution prepared by mixing solutions of Na₂HPO₄ and NaH₂PO₄ under sonication for two min. Every sample of 25 mL performed in a beaker of 30 mL was put at a fixed distance of the light source, as shown in the new Figure S1 added now as supplementary information. Prior to irradiation, the suspension was magnetically stirred for 30 min to establish an adsorption/desorption equilibrium.

The suspensions were irradiated by Simulator Solar (Sciencetech SS 150W Ltd., London, ON, Canada), the luminance of the light source over the reactant solution was 1000 W/cm². All samples were constantly magnetically stirring to ensure a high level of homogeneity of the photocatalyst in the suspension. Samples of 0.35 mL were extracted every 30 min under uninterrupted irradiation. The MB concentration after equilibration was regarded as the initial concentration (C₀) and was monitored by its absorption in the UV-vis spectra of the solution (Shimadzu UV-2450, Shimadzu Corporation, Kyoto, Japan) using nanopure water as a reference.

3.5. Characterization

XRD analyses of the products were performed using a Bruker D8 Advance (Cu K α λ = 1.5418 Å). The SEM and TEM images were obtained by using an EVO MA 10 ZEISS and TEM Hitachi model HT7700 microscopes, respectively. TEM analysis was carried out by dispersing the powder products as slurry in ethanol before drying them on a Cu grid. The diffuse reflectance UV-vis spectra were recorded in the range of 200–800 nm, at a medium scan rate and a slit of 0.1 nm at room temperature, using a Shimadzu UV-2450 spectrometer. Barium sulfate was used in all cases as a reference material. Reflectance measurements were converted to absorption spectra using the Kubelka-Munk function.

4. Conclusions

The prepared nanocomposites enhance the photocatalytic activity in the degradation of methylene blue under UV-vis light. The efficacy of the products described as catalysts for the photo-oxidation of organic pollutants is associated with properties of hybrid nanocomposites. The nanotubes of VOx can act as electron mediators to effectively inhibit the recombination of photogenerated electron/hole pairs and optimize the absorption of visible light. The study with trapping reagents demonstrates that the •OH and O₂•⁻ radicals are the species primarily responsible for photocatalytic oxidative reactions. The products are recyclable and are seen as potentially useful for environmental remediation issues.

Supplementary Materials: The following are available online at <http://www.mdpi.com/2073-4344/8/2/93/s1>, Figure S1: Experimental system of the beaker with 25 mL of MB under solar simulated light, Table S1: Diffraction data and distances corresponding to (001) reflections.

Acknowledgments: Work supported by UTEM, UCh, FONDECYT 1151189; Basal Financing Program CONICYT, FB0807 (CEDENNA). CMST acknowledges the support from the Spanish MINECO projects PHENTOM (FIS2015-70862-P), Severo Ochoa (SEV-2013-0295) and from the CERCA Programme/Generalitat de Catalunya.

Author Contributions: Eglantina Benavente and Guillermo Gonzalez conceived and designed the experiments. Eglantina Benavente and Sindy Davis performed the experiments. Eglantina Benavente, Clivia Sotomayor-Torres and Guillermo Gonzalez analyzed the data and discussed results. Eglantina Benavente, Daniel Navas, Marjorie Segovia and Sindy Davis contributed reagents/materials/analysis tools. Eglantina Benavente wrote the paper.

Conflicts of Interest: The authors declare no conflict of interest.

References

1. Hoffmann, M.; Martin, S.; Choi, W.; Bahnemann, D. Environmental applications of semiconductor photocatalysis. *Chem. Rev.* **1995**, *95*, 69–96. [[CrossRef](#)]

2. Rajeshwar, K.; Thomas, A.; Janaky, C. Photocatalytic activity of inorganic semiconductor surfaces: Myths, hype, and reality. *J. Phys. Chem. Lett.* **2015**, *6*, 139–147. [[CrossRef](#)] [[PubMed](#)]
3. Jassby, D.; Farnar Budariz, J.; Wiesner, M. Impact of Aggregate Size and Structure on the Photocatalytic Properties of TiO₂ and ZnO Nanoparticles. *Environ. Sci. Technol.* **2012**, *46*, 6934–6941. [[CrossRef](#)] [[PubMed](#)]
4. Kudo, A.; Miseki, Y. Heterogeneous photocatalyst materials for water splitting. *Chem. Soc. Rev.* **2009**, *38*, 253–278. [[CrossRef](#)] [[PubMed](#)]
5. Wang, Z. Zinc oxide nanostructures: Growth, properties and applications. *Phys. Condens. Matter* **2004**, *16*, R829–R858. [[CrossRef](#)]
6. Tian, C.; Zhang, Q.; Wu, A.; Jiang, M.; Liang, Z.; Jiang, B.; Fu, H. Cost-effective large-scale synthesis of ZnO photocatalyst with excellent performance for dye photodegradation. *Chem. Commun.* **2012**, *48*, 2858–2860. [[CrossRef](#)] [[PubMed](#)]
7. Udayabhanu; Nagaraju, G.; Nagabhushana, H.; Basavaraj, R.; Raghu, G.; Suresh, D.; Rajanaika, H.; Sharma, S. Green, nonchemical route for the synthesis of ZnO superstructures, evaluation of its applications toward photocatalysis, photoluminescence, and biosensing. *Cryst. Growth Des.* **2016**, *16*, 6828–6840. [[CrossRef](#)]
8. Uddin, T.; Nicolas, Y.; Olivier, C.; Toupance, T.; Servant, L.; Müller, M.; Kleebe, H.J.; Ziegler, J.; Jaegermann, W. Nanostructured SnO₂–ZnO heterojunction photocatalysts showing enhanced photocatalytic activity for the degradation of organic dyes. *Inorg. Chem.* **2012**, *51*, 7764–7773. [[CrossRef](#)] [[PubMed](#)]
9. Kayaci, F.; Vempati, S.; Ozgit-Akgun, C.; Donmez, I.; Biyikli, N.; Uyar, T. Selective isolation of the electron or hole in photocatalysis: ZnO–TiO₂ and TiO₂–ZnO core–shell structured heterojunction nanofibers via electrospinning and atomic layer deposition. *Nanoscale* **2014**, *6*, 5735–5745. [[CrossRef](#)] [[PubMed](#)]
10. Adhikari, S.; Sarkar, D.; Madras, G. Highly efficient WO₃–ZnO mixed oxides for photocatalysis. *RSC Adv.* **2015**, *5*, 11895–11904. [[CrossRef](#)]
11. Jiang, J.; Zhang, X.; Sun, P.; Zhang, L. ZnO/BiOI heterostructures: Photoinduced charge-transfer property and enhanced visible-light photocatalytic activity. *J. Phys. Chem. C* **2011**, *115*, 20555–20564. [[CrossRef](#)]
12. Baek, M.; Kim, E.J.; Hong, S.W.; Kim, W.; Yong, K. Environmentally benign synthesis of CuInS₂/ZnO heteronanorods: Visible light activated photocatalysis of organic pollutant/bacteria and study of its mechanism. *Photochem. Photobiol. Sci.* **2017**, *12*, 1792–1800. [[CrossRef](#)] [[PubMed](#)]
13. Chabri, S.; Dhara, A.; Show, B.; Adak, D.; Sinha, A.; Mukherje, N. Mesoporous CuO–ZnO p–n heterojunction with high specific surface area for enhanced photocatalysis and electrochemical sensing. *Catal. Sci. Technol.* **2016**, *6*, 3238–3252. [[CrossRef](#)]
14. Zou, C.; Rao, Y.; Alyamani, A.; Chu, W.; Chen, M.; Patterson, D.; Emanuelsson, E.; Gao, W. Heterogeneous lollipop-like V₂O₅/ZnO array: A promising composite nanostructure for visible light photocatalysis. *Langmuir* **2010**, *26*, 11615–11620. [[CrossRef](#)] [[PubMed](#)]
15. Haber, J. Fifty years of my romance with vanadium oxide catalysts. *Catal. Today* **2009**, *142*, 100–113. [[CrossRef](#)]
16. Zhou, X.; Wu, G.; Gao, G.; Wang, J.; Yang, H.; Wu, J.; Shen, J.; Zhou, B.; Zhang, Z. Electrochemical performance improvement of vanadium oxide nanotubes as cathode materials for lithium ion batteries through ferric ion exchange technique. *J. Phys. Chem. C* **2012**, *116*, 21685–21692. [[CrossRef](#)]
17. Livage, J. Hydrothermal synthesis of nanostructured vanadium oxides. *Materials* **2010**, *3*, 4175–4195. [[CrossRef](#)] [[PubMed](#)]
18. Wang, J.; Pan, X.; Zhuang, G.; Lu, X. Computational catalysis in nanotubes. *Catalysis* **2014**, *26*, 109–160.
19. Baker, D.; Kamat, P. Photosensitization of TiO₂ nanostructures with CdS quantum dots: Particulate versus tubular support architectures. *Adv. Funct. Mater.* **2009**, *19*, 805–811. [[CrossRef](#)]
20. Tauc, J.; Menth, A. States in the gap. *J. Non-Cryst. Solids* **1972**, *8–10*, 569–585. [[CrossRef](#)]
21. Awasthi, G.; Adhikari, S.; Ko, S.; Kim, H.; Park, C.; Kim, C. Facile synthesis of ZnO flowers modified graphene like MoS₂ sheets for enhanced visible-light-driven photocatalytic activity and antibacterial properties. *J. Alloys Compd.* **2016**, *682*, 208–215. [[CrossRef](#)]
22. Li, Y.; Li, X.; Li, J.; Yin, Y. Photocatalytic degradation of methyl orange by TiO₂-coated activated carbon and kinetic study. *Water Res.* **2006**, *40*, 1119–1126. [[CrossRef](#)] [[PubMed](#)]
23. Benavente, E.; Maldonado, C.; Devis, S.; Díaz, L.; Lozano, H.; Sotomayor-Torres, C.; González, G. A hybrid organic-inorganic layered TiO₂ based nanocomposite for sunlight photocatalysis. *RSC Adv.* **2016**, *6*, 18538–18541. [[CrossRef](#)]
24. Xu, Y.; Schoonen, M.A. The absolute energy positions of conduction and valence bands of selected semiconducting minerals. *Am. Mineral.* **2000**, *85*, 543–556. [[CrossRef](#)]

25. Dong, F.; Sun, Y.; Fu, M. Enhanced visible light photocatalytic activity of V₂O₅ cluster modified n-doped TiO₂ for degradation of toluene in air. *Int. J. Photoenergy* **2012**, *10*, 1–10. [[CrossRef](#)]
26. Yang, X.; Fu, H.; An, X.; Jiang, X.; Yu, A. Synthesis of V₂O₅@TiO₂ core-shell hybrid composites for sunlight degradation of methylene blue. *RSC Adv.* **2016**, *6*, 34103–34109. [[CrossRef](#)]
27. Zhang, N.; Chen, D.; Niu, F.; Wang, S.; Qin, L.; Huang, Y. Enhanced visible light photocatalytic activity of Gd doped BiFeO₃ nanoparticles and mechanism insight. *Sci. Rep.* **2016**, *6*, 26467. [[CrossRef](#)] [[PubMed](#)]
28. Wang, H.; Zhao, Y.; Su, Y.; Li, T.; Yao, M.; Qin, C. Fenton-like degradation of 2,4-dichlorophenol using calcium peroxide particles: Performance and mechanisms. *RSC Adv.* **2017**, *7*, 4563–4571. [[CrossRef](#)]
29. Segovia, M.; Lemus, K.; Moreno, M.; Santa Ana, M.; González, G.; Ballesteros, B.; Sotomayor, C.; Benavente, E. Zinc oxide/carboxylic acid lamellar structures. *Mater. Res. Bull.* **2011**, *46*, 2191–2195. [[CrossRef](#)]
30. O'Dwyer, C.; Lavayen, V.; Newcomb, S.; Santa Ana, M.; Benavente, E.; González, G.; Sotomayor-Torres, C. Vanadate conformation variations in vanadium pentoxide nanostructures. *J. Electrochem. Soc.* **2007**, *154*, K29–K35. [[CrossRef](#)]



© 2018 by the authors. Licensee MDPI, Basel, Switzerland. This article is an open access article distributed under the terms and conditions of the Creative Commons Attribution (CC BY) license (<http://creativecommons.org/licenses/by/4.0/>).